Hydrogen migration in polycrystalline silicon

N. H. Nickel, W. B. Jackson, and J. Walker
Xerox Palo Alto Research Center, 3333 Coyote Hill Road, Palo Alto, California 94304
(Received 13 March 1995; revised manuscript received 1 November 1995)

Hydrogen migration in solid-state crystallized and low-pressure chemical-vapor-deposited (LPCVD) polycrystalline silicon (poly-Si) was investigated by deuterium diffusion experiments. The concentration profiles of deuterium, introduced into the poly-Si samples either from a remote D plasma or from a deuterated amorphous-silicon layer, were measured as a function of time and temperature. At high deuterium concentrations the diffusion was dispersive depending on exposure time. The dispersion is consistent with multiple trapping within a distribution of hopping barriers. The data can be explained by a two-level model used to explain diffusion in hydrogenated amorphous silicon. The energy difference between the transport level and the deuterium chemical potential was found to be about 1.2–1.3 eV. The shallow levels for hydrogen trapping are about 0.5 eV below the transport level, while the deep levels are about 1.5–1.7 eV below. The hydrogen chemical potential μ_H decreases as the temperature increases. At lower concentrations, μ_H was found to depend markedly on the method used to prepare the poly-Si, a result due in part to the dependence of crystallite size on the deposition process. Clear evidence for deuterium deep traps was found only in the solid-state crystallized material. The LPCVD-grown poly-Si, with columnar grains extending through the film thickness, displayed little evidence of deep trapping, and exhibited enhanced D diffusion. Many concentration profiles in the columnar LPCVD material indicated complex diffusion behavior, perhaps reflecting spatial variations of trap densities, complex formation, and/or multiple transport paths. Many aspects of the diffusion in poly-Si are consistent with diffusion data obtained in amorphous silicon.

I. INTRODUCTION

Polycrystalline silicon (poly-Si) has attracted a great deal of interest as an active material in photovoltaic devices and large area applications such as thin-film transistors. However, to obtain technologically useful material, grain-boundary defects in poly-Si must be passivated. Commonly, this is achieved by exposing poly-Si to a hydrogen plasma at elevated temperatures. Hydrogen introduced into poly-Si diffuses in the positive charged state (H^+) and enhances the electrical conductivity during the exposure.[1] The hydrogenation results in a decrease of the defect density, thereby improving the electrical properties of the poly-Si films and devices.[2–5] As a function of the hydrogenation time, the dangling-bond density decreases to a residual saturation value that strongly depends on the passivation temperature. The total H concentration in hydrogen-passivated polycrystalline silicon (poly-Si:H) exceeds the dangling-bond spin density by more than two orders of magnitude.[6]

Until recently there was no evidence of any deleterious aspects in poly-Si due to the presence of hydrogen. Recently, however, it has been demonstrated that hydrogen is directly involved in various phenomena: (i) Illumination produces metastable Si dangling bonds in hydrogenated poly-Si. It is believed that hydrogen atoms, migrating as a result of illumination, cause the rupture of strained Si-Si bonds in the grain-boundary regions generating spin-active defects.[7] (ii) A cooling-rate-dependent metastable change occurs in the dc dark conductivity of poly-Si:H.[8] Hydrogen becomes trapped in the bond-center position of strained Si-Si bonds donating its electron which results in an increase of the electrical conductivity. This complex has recently been identified as a donor state in crystalline silicon.[9–11] (iii) Prolonged exposure of intrinsic poly-Si to monatomic hydrogen at elevated temperatures causes the formation of acceptorlike states which leads to electrical type conversion. The newly created acceptor states are stable up to 350 °C.[1] These hydrogen-induced deleterious effects in poly-Si and the defect passivation are governed by diffusion kinetics. Therefore, because the hydrogenation process is both essential and leads to undesirable effects, it is important to understand hydrogen transport and binding in poly-Si.

In this paper we investigate hydrogen transport in differently prepared poly-Si films by analyzing deuterium and hydrogen diffusion depth profiles measured by secondary-ion-mass spectrometry (SIMS). The H diffusion was studied as a function of time, temperature, and concentration, using either a remote deuterium plasma or a deuterated amorphous-silicon layer (solid source). We find that the hydrogen diffusion properties depend strongly on the deuterium source and on the host material.

The paper is organized as follows. Section II briefly describes the sample preparation and the experimental techniques used to hydrogenate and characterize the specimens. Deuterium and hydrogen concentration profiles obtained by secondary-ion-mass spectrometry are presented in Sec. III. In Sec. IV we discuss the implications of the data for hydrogen transport in poly-Si and the influence of the microscopic structure on the diffusion process. Finally, Sec. V summarizes the main conclusions of this work.

II. EXPERIMENT

A. Samples

The experiments described in this paper were performed on two kinds of undoped polycrystalline silicon films. The

0163-1829/96/53(12)/7750(12)/$10.00 © 1996 The American Physical Society

first set of poly-Si films was deposited by low-pressure chemical vapor deposition (LPCVD) at 625 °C to a thickness of 0.55 μm. Cross-sectional transmission electron microscopy revealed that this material was composed of columnar grains with a smaller grain size near the substrate as compared to the bulk. The average grain diameter is 15 nm, and the length of the grains is only limited by the film thickness. The second set of poly-Si films was prepared by solid-state crystallization (SSC) of 0.3- and 0.55-μm-thick LPCVD *amorphous silicon* at 600 °C. In this material the grain boundaries are randomly distributed, and the average grain size is 120 nm. Both materials were deposited on quartz and on single-crystal silicon wafers with a thin thermal oxide, 10 nm thick.

B. Hydrogen passivation

Hydrogen (deuterium) was introduced into the samples from two distinct sources: remote plasma and diffusion from a solid-state layer. The hydrogen passivation by remote plasma was accomplished through the following steps. The samples were given a metal-oxide-semiconductor grade detergent cleaning, and the native oxide was removed with dilute HF to avoid a barrier to hydrogen incorporation. Then the specimens were exposed to monatomic hydrogen produced in an optically isolated remote hydrogen plasma. For SIMS analysis, deuterium was used as a readily identifiable isotope which duplicates hydrogen chemistry. In the subsequent discussion, the term hydrogenation will be used interchangeably with deuteration because no significant different transport has been found for the two isotopes. Solid-state crystallized and LPCVD-grown undoped poly-Si films were simultaneously exposed to monatomic deuterium varying time periods and temperatures. During post-deuteration the concentration of monatomic D in the plasma is constant, and was estimated to be $\approx 10^{15}$ cm^{-3} using electron paramagnetic resonance measurements.[12]

Solid-state or layer hydrogenation was accomplished using the following protocol. After removing the native oxide from both SSC and LPCVD poly-Si films, a 0.1-μm-thick deuterated amorphous silicon (a-Si:H:D) layer was deposited at 150 °C by diluting silane with 20% deuterium in the gas phase. The a-Si:H:D layer was sealed with a 0.5-μm-thick a-Si:H capping layer. The structure was then annealed at various temperatures, causing the deuterium to diffuse into the poly-Si. The capping layer prevented a significant deuterium loss during annealing.

In the above experiments, a change in temperature was found to affect the D concentration as well as the diffusion. In order to separate the concentration dependence from the temperature dependence, the D concentration at a fixed temperature was attenuated using two different methods: (i) Two samples were simultaneously hydrogenated. One sample was mounted with the poly-Si layer facing away from the remote plasma and toward the sample holder. A 1-mm gap between the sample holder and the sample was provided by two ceramic pillars. The H concentration at the poly-Si surface was attenuated by the recombination of H on the surface of the sample holder. A sample with the poly-Si film facing the remote plasma served as a control. (ii) A 10-nm-thick silicon-oxide layer was deposited on top of the poly-Si film.

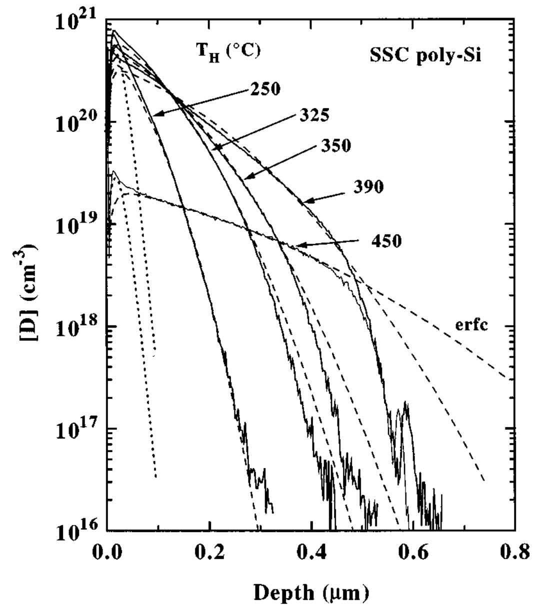

FIG. 1. Deuterium concentration depth profiles in solid-state crystallized poly-Si (solid lines). The specimens were exposed to monatomic deuterium for 60 min at the indicated temperatures. The dashed lines depict a least-squares fit to the convolution of an erfc with the SIMS depth resolution function [Eq. (1)]. The dotted curves indicate the accumulation of D close to the sample surface.

The concentration of monatomic D is attenuated because the activated H fails to penetrate the oxide, thereby reducing the concentration of atomic H in the top surface of the poly-Si for a fixed temperature. This results in a decrease of the surface concentration of monatomic D in the specimen. Using the above procedures, the effect of changes in concentration could be adjusted independently of temperature.

The deuterium concentration profiles were measured by SIMS using a Cs^+-ion beam. A standard crystalline silicon sample implanted with a deuterium dose of 1×10^{14} cm^{-2} was used to calibrate the deuterium concentrations. The absolute concentration values are accurate to within a factor of 2, but the relative precision when comparing two profiles is much better. The depth scales were obtained by measuring the depth of the sputtered craters using a mechanical stylus.

III. RESULTS

The results presented in this section consist of the following experimental matrix formed by varying the following parameters: the type of poly-Si (SSC or LPCVD), deuteration source (remote plasma or diffusion from a solid source), temperature, time, and concentration. Section III A presents results for diffusion from a plasma, and Sec. III B presents the results for diffusion from a layer. Within each of these sections, the effect of the type of poly-Si, and the time and temperature are presented.

A. Diffusion from a plasma

1. Solid-state crystallized (SSC) poly-Si

Figure 1 shows typical D concentration profiles in solid-state crystallized (SSC) poly-Si after an exposure to mon-

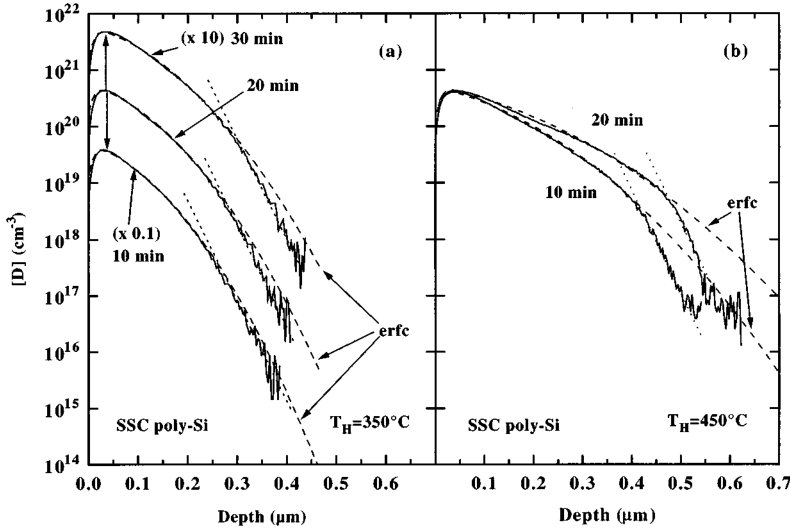

FIG. 2. Time dependence of deuterium depth profiles in solid-state crystallized poly-Si exposed to monatomic D (a) at 350 °C (note: offset for clarity) and (b) at 450 °C. The dashed lines depict a least-squares fit to Eq. (1). The dotted lines indicate the exponential decays with a characteristic length of $x_0 = 24.3$ nm for all profiles.

atomic deuterium at various indicated temperatures for 60 min. With increasing temperature the deuterium concentration in the bulk of the specimens increases, while the D concentration at the surface (the depth equals 0) decreases from 1×10^{21} cm^{-3} at 250 °C to 2.6×10^{19} cm^{-3} at 450 °C. The D surface concentration C_0, and the effective diffusion coefficient D_{eff}, were obtained from least-squares fits of the data to the convolution of a complementary error function and the resolution function of the SIMS analysis:[13]

$$C_D(x,t) = C_0\left[\mathrm{erfc}\left(\frac{x}{S(t)}\right) + R_{\mathrm{SIMS}}\right], \qquad (1)$$

with $S(t) = (4D_{\mathrm{eff}}t)^{1/2}$ and t is the diffusion time. For diffusion from a deuterium plasma, R_{SIMS} is given by

$$R_{\mathrm{SIMS}} = \exp\left(-\frac{x}{x_R}\right)\left\{\exp\left(\frac{S^2(t)}{4x_R^2}\right)\left[\mathrm{erfc}\left(\frac{S(t)}{2x_R} - \frac{x}{S(t)}\right) - \mathrm{erfc}\left(\frac{S(t)}{2x_R}\right)\right] - 1\right\}, \qquad (2)$$

with a SIMS depth resolution of $x_R = 8$ nm. Within the first 1000 Å the concentration profiles exhibit a surface peak indicated by the dotted curves in Fig. 1. For a depth greater than 1000 Å and at high D concentrations the fits (dashed curves in Fig. 1) are in good agreement with the data, indicating that the D transport can be described by a single diffusion coefficient. However, at concentrations below $\approx 4\times10^{18}$ cm^{-3} the diffusion profiles deviate from the fits, and decay exponentially with depth. This deviation increases as deuterium diffuses deeper into the sample.

The time dependence of the deuterium diffusion in solid-state crystallized poly-Si for two temperatures is shown in Fig. 2 (solid curves), and fits to Eq. (1) are superimposed (dashed lines). Independent of the deuteration temperature T_{H}, and the diffusion time, all deuterium depth profiles deviate from a complementary error function at a concentration of $4-8\times10^{18}$ cm^{-3}. The dotted lines in Fig. 2 represent least-squares fits to an exponential decay with a slope of $x_0 = 24.3$ nm which is independent of exposure time and temperature. The curves of Fig. 2(a) are shifted vertically for clarity. With increasing exposure time D diffuses deeper into the sample, and increases the deuterium concentration in the bulk. Since the slope of the exponential decay remains constant, the gap between the data and erfc fit increases. A similar diffusion behavior has previously been reported in amorphous silicon (a-Si).[14–16] As will be discussed below in Sec. IV, the kink between the erfc and an exponential decay in the diffusion depth profiles occurs when the deuterium concentration equals the trap density.

By fitting the high concentration portion of the profiles in Figs. 1 and 2, the effective diffusion coefficient D_{eff} was determined as a function of plasma exposure time and temperature. In Fig. 3 the effective diffusion coefficient is plotted versus $1/T$ as indicated by the open triangles. The effective diffusion coefficient D_{eff} has an apparent activation energy of 0.63 eV. This diffusion activation energy is similar to the 0.8-eV activation energy observed for diffusion from a plasma source into hydrogenated amorphous silicon, and is different from the diffusion from a layer.[13] The dependence of D_{eff} on hydrogenation time and temperature is shown by the open triangles in Fig. 4. Because the scales are log-log, D_{eff} exhibits a power-law dependence on deuteration time. The data was fitted to the form[17,18]

$$D_{\mathrm{eff}} \approx D_0(\omega t)^{-(1-\beta)} \qquad (3)$$

where D_0 is a constant, ω is an attempt frequency, and $\beta = T/T_0$ is the dispersion parameter. T is the measurement temperature, and T_0 is the characteristic disorder temperature discussed below. The solid lines in Fig. 4 depict the results of the fits of Eq. (3). In summary, the data presented above demonstrate that diffusion of deuterium in SSC poly-Si exhibits an activated and dispersive character.

It is important for understanding microscopic diffusion processes to separate the concentration dependence of the diffusion from the temperature dependence. In previous experiments a change of the deuterium surface concentration always occurred in conjunction with a temperature change.

Figures 5 and 6 illustrate the concentration dependence of the deuterium diffusion. In Fig. 5 the curve labeled "normal" represents a typical depth profile obtained after a 20-min exposure to monatomic D at 350 °C. The lower curve was

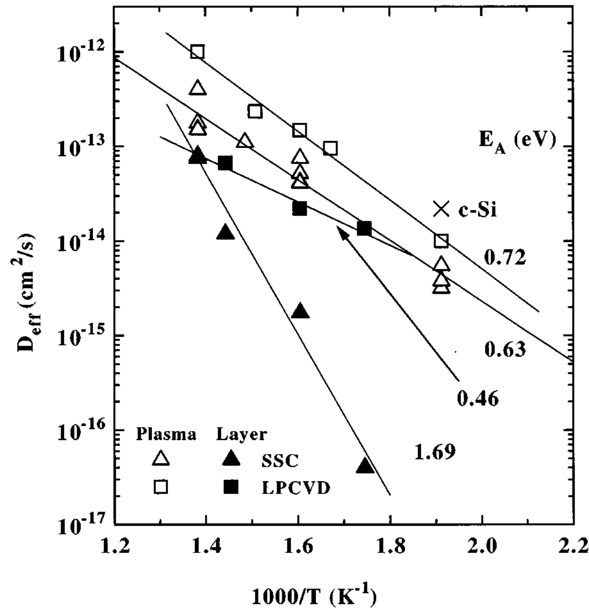

FIG. 3. Diffusion coefficient as a function of the reciprocal temperature for diffusion from a plasma (open symbols) and a solid source (solid symbols). The triangles represent solid-state crystallized poly-Si and the squares were obtained on LPCVD-grown poly-Si films. The cross represents the diffusion coefficient of c-Si which was obtained from the high-D concentration part of the depth profile shown in Fig. 10. The activation energies were obtained from the slopes of the lines and are indicated in the figure.

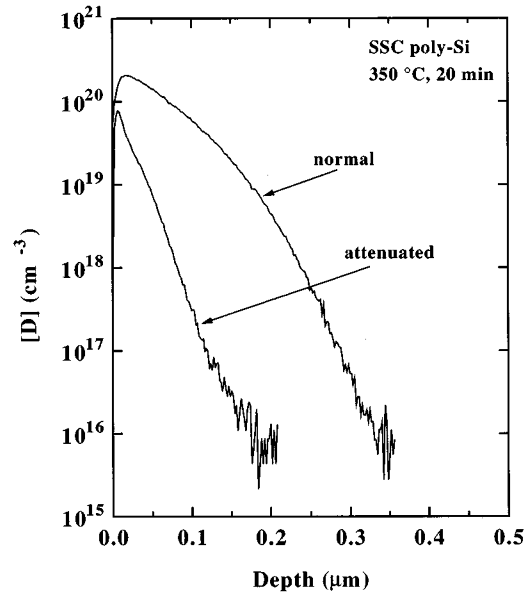

FIG. 5. Deuterium depth profiles in solid-state crystallized poly-Si after an exposure to monatomic D at 350 °C for 20 min. The lower curve was obtained by attenuating the D surface concentration and the upper curve displays the D concentration profile after a normal plasma exposure.

obtained exposing the specimen under identical conditions, but attenuating the flux of monatomic D into the sample by mounting it upside down on ceramic pillars. In this case the depth profile exhibits a simple exponential decay with a decay length of $\approx$19.5 nm. An even stronger attenuation was achieved by depositing a 10-nm thick SiO_2 layer on top of the poly-Si film. This causes the surface D concentration to decrease by almost three orders of magnitude for identical deuteration conditions (Fig. 6). As observed in Fig. 5, the profiles deviate from a complementary error function and decay exponentially with depth with a decay length of $\approx$22 nm. The exponential decay is not due to the SIMS depth resolution, which is about 8 nm. Moreover, the decay length

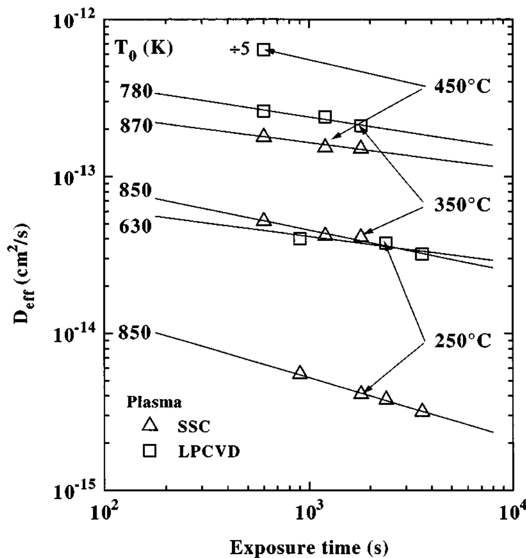

FIG. 4. Time dependence of the effective diffusion coefficient D_{eff} for various temperatures. The open triangles correspond to solid-state crystallized poly-Si, and the open squares were obtained on LPCVD-grown poly-Si films. The lines represent a least-squares fit to the expression $D_{\text{eff}} \approx D_0(\omega t)^{-(1-T/T_0)}$. The values obtained for the T_0 are indicated.

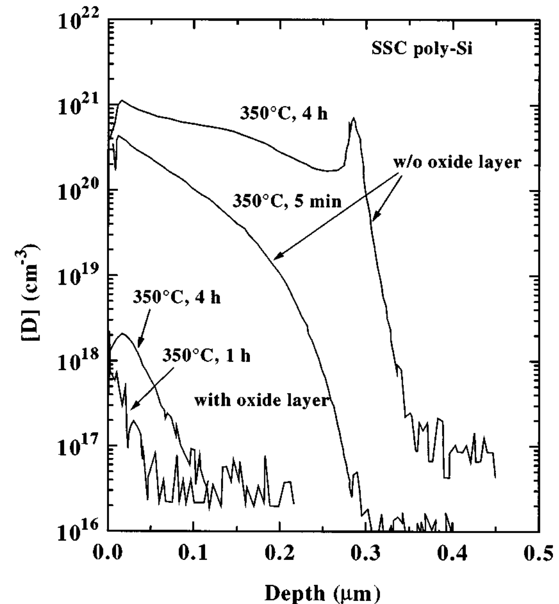

FIG. 6. Deuterium depth profiles in solid-state crystallized poly-Si with and without a 10-nm-thick SiO_2 layer. The specimens were exposed to monatomic D at 350 °C for the indicated times.

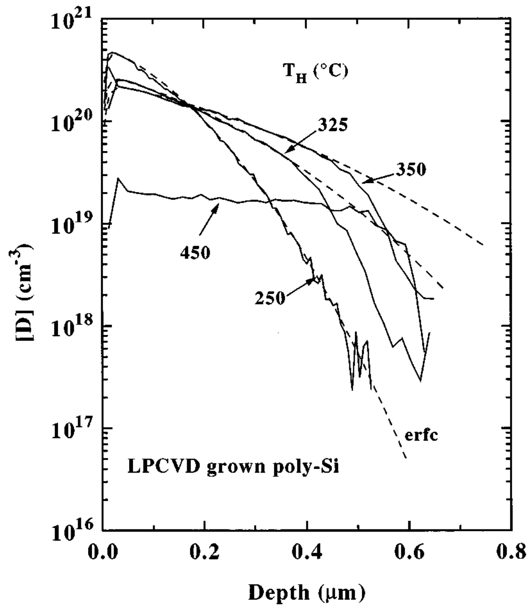

FIG. 7. Deuterium concentration depth profiles in LPCVD-grown polycrystalline silicon films composed of columnar grains (solid lines). The specimens were exposed to monatomic deuterium for 60 min at the indicated temperatures. The dashed lines depict a least-squares fit to Eq. (1). The poly-Si/substrate interface is located at a depth of 0.55 μm.

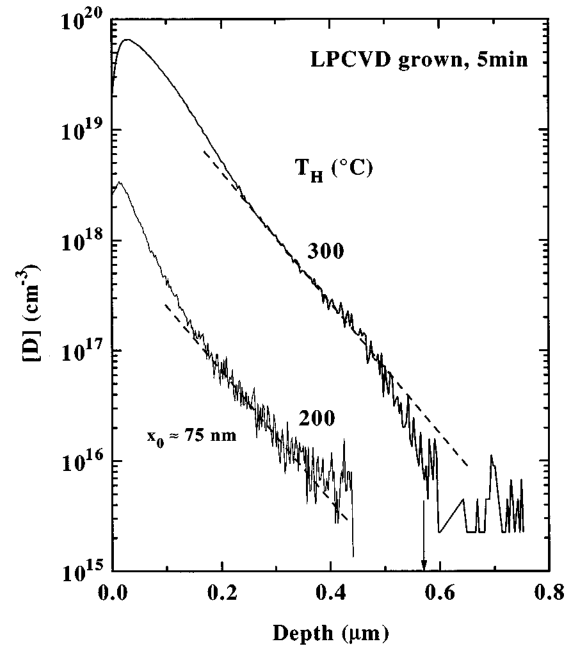

FIG. 8. Deuterium concentration depth profiles in LPCVD-grown polycrystalline silicon (solid curves) after an exposure to monatomic deuterium at 200 and 300 °C, respectively, for 5 min. The dashed curves represent least-squares fits to an exponential decay with a characteristic decay length $x_0 \approx 75$ nm. Note the enhanced deuterium concentration in the surface region.

is consistent with the results of Figs. 1 and 2, where trap-dominated diffusion was observed for deuterium concentrations less than $4-8\times10^{18}$ cm^{-3}. In both cases the plasma attenuation causes a decrease of the D surface concentration which is accompanied by a decrease of the diffusion coefficient (e.g., in Fig. 5 $D_{\rm eff}$ decreased from 6.2×10^{-14} to 6.7×10^{-15} cm^2/s). For a concentration-independent diffusion coefficient the reduction of the surface concentration would not affect $D_{\rm eff}$. Thus, from the above data, it can be concluded that the concentration dependence of the diffusion coefficient is quite important.

2. LPCVD poly-Si

The effect of the crystallite structure on the diffusion is investigated by repeating the experiments using LPCVD-grown poly-Si. Deuterium depth profiles obtained on LPCVD-grown poly-Si films after an exposure to monatomic D for 60 min are plotted in Fig. 7. Comparing the data to the diffusion profiles obtained on SSC poly-Si shows that the deuterium diffusion in LPCVD-grown poly-Si is enhanced. At low hydrogenation temperatures ($T_{\rm H}=250$ °C) the deuterium concentration at the sample surface (the depth equals 0) is $C_0=4.2\times10^{20}$ cm^{-3}. With increasing temperature the deuterium concentration decreases and becomes nearly constant with depth at $T_{\rm H}=450$ °C. The dashed curves in Fig. 7 represent least-squares fits of the data to Eq. (1), and fit the data well. As observed in the SSC poly-Si for D concentrations below $\approx4\times10^{19}$ cm^{-3}, the depth profiles deviate from the fit ($T_{\rm H}>250$ °C), and the D concentration decays approximately exponentially with depth. However, in contrast to SSC poly-Si, this deviation occurs when the D reaches the substrate. The deviation is therefore due to the effect of the substrate on the diffusion profile at a depth of 0.55 μm, and does not reflect the presence of deep H traps.

The influence of the substrate on the deuterium depth profiles can be avoided by decreasing the exposure time. Two LPCVD specimens were exposed for 5 min to monatomic D at 200 and 300 °C, respectively. The concentration profiles are represented by the solid curves in Fig. 8. Shorter deuteration times reveal an interesting feature in the D depth profiles. At a depth of ≈0.2 μm the profiles exhibit a kink which becomes more pronounced at lower deuteration temperatures. These depth profiles cannot be described by a single diffusion process. The high concentration region appears to be distinct from the exponential region at lower concentrations. This observation is similar to the data obtained in SSC poly-Si, where the surface D peak is only slightly smaller than the erfc region (dotted lines in Fig. 1). The dashed lines in Fig. 8 represent least-squares fits to an exponential decay with a slope of ≈75 nm independent of the temperature or time, suggesting that the low concentration region represents H trapping onto deep traps. The deviation of the fit observed in the specimen which was deuterated at 300 °C is caused by the influence of the poly-Si/substrate interface (indicated by an arrow) on the diffusion profile even for an exposure time of only 5 min. The enhanced hydrogen diffusion in LPCVD-grown poly-Si is again quite apparent.

Fitting the high-concentration regions of the deuterium diffusion profiles in Figs. 7 and 8 to Eq. (1) yields the effective diffusion coefficient $D_{\rm eff}$ as a function of plasma exposure time and temperature. The effect of temperature on $D_{\rm eff}$ in LPCVD-grown poly-Si is presented by the open squares in Fig. 3. $D_{\rm eff}$ is thermally activated with $E_a=0.72$

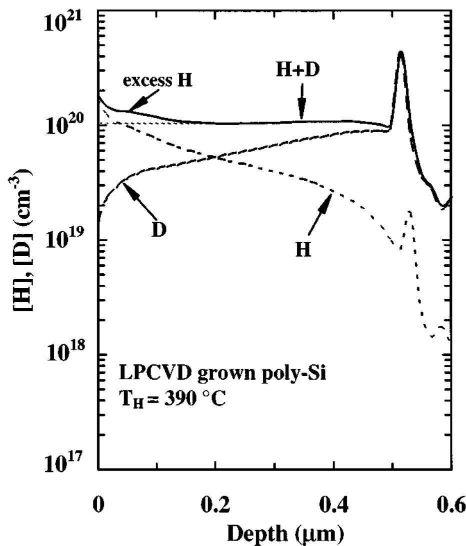

FIG. 9. Hydrogen (dotted curve), deuterium (dashed curve), and hydrogen *plus* deuterium depth profiles (solid curve) in LPCVD-grown polycrystalline silicon. Deuterium was introduced through a sequence of five 60-min exposures at 390 °C. Then the specimens were exposed to monatomic H for 1 h. Prior to each plasma exposure, the oxide layer was removed with dilute HF.

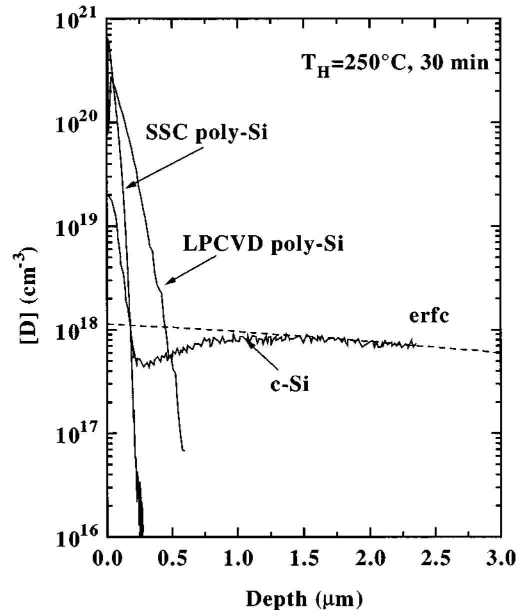

FIG. 10. Deuterium concentration profiles as a function of the sample depth in single-crystal silicon, solid-state crystallized, and LPCVD-grown poly-Si. The specimens were exposed simultaneously to a remote deuterium plasma at $T_H = 250$ °C for 30 min. The dashed line represents a least-squares fit to a complementary error function.

eV, comparable to that found for the SSC poly-Si. In Fig. 4 the time dependence of D_{eff} for LPCVD-grown poly-Si is shown by the open squares for three passivation temperatures. The time dependence of the LPCVD material is quite similar to that of SSC material. However, at all deuteration temperatures the effective diffusion coefficients are larger in LPCVD-grown poly-Si than in the SSC material. A comparison of diffusion in LPCVD and SSC poly-Si indicates that the crystalline structure of the material makes a large difference. On the other hand, independent of the crystallite structure and the deuteration temperature, D_{eff} decreases with increasing exposure time.

One might expect that the number of trapping sites is a function of the grain boundaries which changes markedly between the two materials. The effect of the number of trapping sites on the diffusion was investigated by measuring the effect of prior deuteration on H transport in LPCVD films. In this way the number of traps could be adjusted independently of the crystalline structure. In order to investigate H diffusion in poly-Si:H some specimens were passivated with deuterium through a sequence of five 1-h exposures at 390 °C followed by a 1-h exposure to monatomic H. Prior to each plasma exposure the oxide layer of the specimens was removed with dilute HF. The concentration profiles for hydrogen, deuterium, and hydrogen *plus* deuterium are shown in Fig. 9. In the entire depth of the specimen a significant fraction of deuterium is replaced by hydrogen. The D exchange is more pronounced at the surface (the depth equals 0) where the D concentration decreases by about one order of magnitude. The D loss weakens gradually toward the interface indicated by the peaks in the depth profiles. Despite the deuterium outdiffusion the total H *plus* D concentration (solid curve in Fig. 9) increases over a depth of 0.1 μm by about 35%, indicating that the deuterium loss is over compensated by indiffusing H. The effective diffusion coefficients for both H indiffusion and D outdiffusion were found to be $D_{eff} \approx 3 \times 10^{-13}$ cm^2/s by fitting the data to an erfc. Similar results were obtained by reversing the hydrogenation-deuteration sequence. Moreover, the results are independent of the macroscopic structure of the poly-Si; e.g., LPCVD-grown and SSC poly-Si exhibited similar H and D outdiffusion behavior, though with different values for the diffusion coefficient. The difference in transport behavior between SSC and LPCVD-grown poly-Si is therefore not simply a result of different numbers of traps filled by H.

The effect of substrate structure was further investigated by comparing diffusion in the various forms of poly-Si to diffusion in c-Si under similar conditions. In Fig. 10 deuterium depth profiles measured in SSC and LPCVD-grown poly-Si are compared to depth profiles obtained in c-Si. The specimens were exposed simultaneously to monatomic D from a remote plasma at 250 °C for 30 min. The data in Fig. 10 show that deuterium diffusion in poly-Si is strongly reduced compared to the diffusion in c-Si. These results demonstrate that grain boundaries act as efficient traps for H and D, effectively reducing the diffusivity as was previously suggested by Jackson *et al.*[19] Among the poly-Si samples, the diffusivity in LPCVD-grown poly-Si is larger than in SSC poly-Si. The depth resolution, however, is not high enough to show that accumulation of D in the surface region of the poly-Si samples which is attributed to the formation of hydrogen-stabilized platelets.[20] Of particular interest is the fact that the high concentration diffusion profiles of all the samples are remarkably similar particular for LPCVD-grown poly-Si and c-Si. The slopes of the concentration profiles are similar for D concentrations exceeding 10^{18} cm^{-3}. The c-Si sample possesses a very fast, low concentration component that is not present in the disordered Si samples. At a

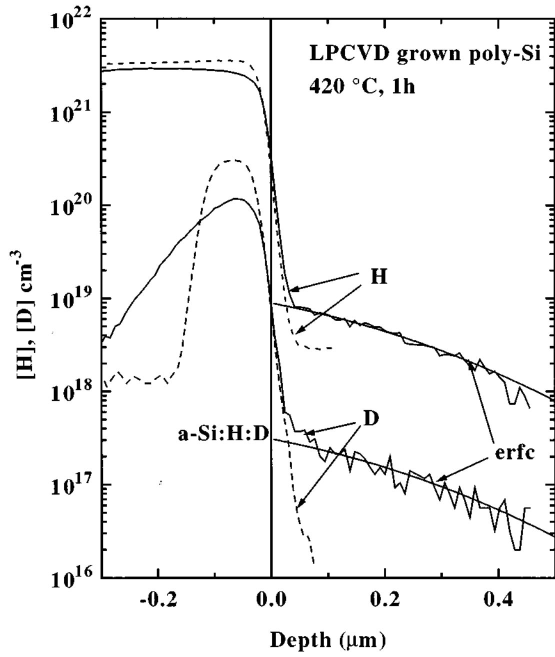

FIG. 11. Diffusion from a deuterated amorphous silicon (a-Si:H:D) layer into unhydrogenated LPCVD-grown poly-Si. Layer diffusion was performed by annealing the specimens at 420 °C for 1 h. The dashed curves illustrate the D and H profiles prior to the diffusion experiment and the solid curves were obtained after annealing. After the diffusion experiment the deuterium and hydrogen profiles decay according to a complementary error function (erfc). A depth of 0 μm marks the interface between a-Si:H:D and poly-Si layer.

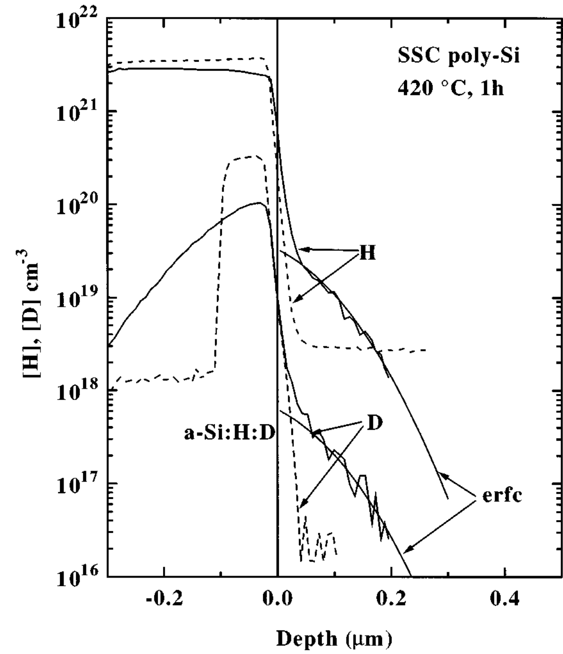

FIG. 12. Diffusion from a deuterated amorphous silicon (a-Si:H:D) layer into unhydrogenated solid-state crystallized poly-Si. For details see Fig. 11.

depth >1 μm the decay of the D concentration follows an erfc (dashed curve). The least-squares fit yielded a D surface concentration of $C_0 = 1.2\times10^{18}$ cm^{-3} and a diffusion coefficient of $D_{\rm eff} = 7.2\times10^{-11}$ cm^2/s which is about 2–3 orders of magnitude larger compared to the diffusion coefficients obtained for low concentration diffusion (full symbols in Fig. 3). Thus, at low concentrations, there is considerable difference between poly-Si and c-Si while, at high concentrations the diffusion is remarkably similar and independent of the form of the silicon lattice.

B. Diffusion from a solid source

Exposure to a remote plasma requires the deuterium to overcome possible surface barriers to enter the samples. Although the surface was kept clean, the buildup of surface species such as oxides during hydrogenation is unavoidable. Such surface layers could affect the transport of deuterium into the sample. Diffusion of deuterium from a solid-state overlayer provides an alternative means for introducing D which could have a different set of barriers for incorporation into the polycrystalline silicon. A comparison of diffusion between D introduced by a remote plasma and from a solid source could reveal such surface-limited processes. Furthermore, because the surface concentration is greatly reduced when deuterium diffuses from a deuterated layer into unhydrogenated poly-Si, the solid source provides an alternative means for studying the concentration dependence of the D transport.

Typical D concentration profiles of a a-Si:H/a-Si:H:D/poly-Si multilayer structure are shown in Figs. 11 and 12 for LPCVD-grown and SSC poly-Si, respectively. The solid line at a depth of 0 indicates the interface between the a-Si:H:D and the poly-Si layers. The dashed curves represent the deuterium and hydrogen depth profiles of *as-prepared* multilayer structures. The exponential decay at the interface is determined by the SIMS depth resolution ($x_0 = 8$ nm) which is limited by the intermixing of material during ion bombardment.[21] The solid curves show the D and H depth profiles after annealing the specimens at 420 °C for 1 h. The effective diffusion coefficient $D_{\rm eff}$ and surface concentration C_0 were obtained by fitting the data to Eq. (1), where $R_{\rm SIMS}$ becomes

$$R_{\rm SIMS} = \exp\left(\frac{S^2(t)}{4x_R^2} - \frac{x}{x_R}\right)\mathrm{erfc}\left(\frac{S(t)}{2x_R} - \frac{x}{S(t)}\right). \qquad (4)$$

The D surface concentration was found to be $\approx 3.5\times10^{17}$ and $\approx 6.5\times10^{17}$ cm^{-3} in LPCVD-grown and SSC poly-Si, respectively. The H surface concentration amounts to $\approx 10^{19}$ and $\approx 3\times10^{19}$ cm^{-3} in LPCVD-grown and SSC poly-Si, respectively. In both materials diffusion becomes appreciable above 300 °C. The resulting hydrogen and deuterium diffusion profiles decay with depth according to a complementary error function, indicating that the total H *plus* D concentration exceeds the number of deep traps (Figs. 11 and 12). It is interesting to note that in the a-Si:H:D layer the H concentration exceeds the D concentration by one order of magnitude. This difference in H and D concentrations is also observed in the poly-Si layers after the diffusion experiments (Figs. 11 and 12). Moreover, similar to diffusion from a plasma, layer diffusion in LPCVD-grown poly-Si is enhanced compared to SSC poly-Si. The pronounced broad-

ening of the D profile toward the surface of the a-Si:H capping layer (at a depth less than 0) is similar to previous investigations of layer diffusion in a-Si:H.[13]

In Fig. 3 the temperature dependence of the diffusion coefficient for diffusion from a solid source is shown by the solid squares and triangles for LPCVD-grown and solid-state crystallized poly-Si, respectively. In LPCVD-grown poly-Si the diffusion coefficients are about a factor of 3–6 smaller over the entire temperature range compared to diffusion from a plasma source. Surprisingly, however, the apparent activation energy of the diffusivity is independent of the deuterium source ($E_A \approx 0.46$ eV). The temperature dependence of the diffusion coefficient for layer diffusion in SSC poly-Si is represented by the solid triangles in Fig. 3, and exhibits activated behavior with $E_A \approx 1.69$ eV. This value is in good agreement with results reported for solid source diffusion in a-Si:H.[13,22]

IV. DISCUSSION

The data presented in the previous section can be understood in terms of models used to describe diffusion in amorphous and crystalline silicon. Most of the data can be explained by a two-band model described below. The model parameters such as energy depth and trap concentration can be estimated from the temperature and concentration dependence of the hydrogen diffusion. The spatial variation of the concentration profiles provide additional information about the trap concentrations and capture radius, and confirm the parameters derived from the temperature and concentration dependence.

A. Hydrogen density of states

From the experimental data one can determine a number of properties of H transport in poly-Si. Because the H diffusion is similar to that found in amorphous silicon, the results can be interpreted in terms of a hydrogen density-of-states model used to explain transport in a-Si.[13,14] In this model, H transport is assumed to occur between minimum energy positions by surmounting the barrier between sites at a saddle point. In c-Si the saddle point for hydrogen migration occurs 0.2–0.5 eV above the Si-Si bond-center site which was identified as the global minimum for H diffusion[11] (E_M in Fig. 13). The lower number was obtained from first-principles calculations,[11] while the higher value reflects the activation energy of the diffusion coefficient at high temperatures.[23] In contrast to c-Si, polycrystalline silicon is an inhomogeneous material in which identical crystallites are separated by grain boundaries. The degree of disorder commonly present in poly-Si is related to strained Si-Si bonds and dangling-bond defects, which are predominantly confined to these two-dimensional boundaries. The disorder of the host material gives rise to a distribution of barriers between H transport sites. In Fig. 13 the migration saddle point is represented by the energy E_M which is considered to be roughly constant throughout the poly-Si material. Below the barrier energies is a distribution of shallow trapping sites near energy E_{BC} which trap and release the hydrogen as it diffuses through the poly-Si lattice. The H equilibrates within the shallow trap distribution during typical diffusion experiment time scales.

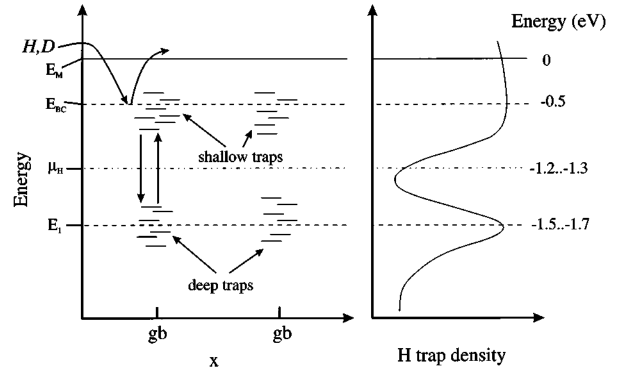

FIG. 13. H traps in poly-Si. E_1 represents deep traps predominantly located at grain boundaries (gb). E_{BC} and E_M denote the energies of the Si-Si bond-center position and the migration saddle point, respectively. The occupation of the various levels is determined by the hydrogen chemical potential μ_H. The hydrogen density-of-states distribution is shown on the right side. Indicated are the energies for E_{BC}, E_1, and μ_H with respect to the migration saddle point for H migration ($E_M = 0$ eV).

Separated in energy from these traps are deep states at energy E_1 which trap and release H on time scales long compared to the diffusion experiments. In equilibrium the hydrogen chemical potential μ_H separates the filled sites from the empty ones. The process of H diffusion can then be described in terms of H trapping and release from the density of binding-site energies over the barrier energies.

For short times, temperatures below about 420 °C, and small changes in H concentration, the density of H traps can be regarded as more or less fixed. The time scales for changes in the density of states are usually long compared to the typical capture and release times, dominating diffusion at temperatures from 200 to 350 °C. However, for large changes in H concentration, long times, and/or temperatures above 420 °C, the concentration of trapping sites can change. Under these conditions, the density of H states, equivalently, the number of sites per unit volume per energy, is therefore a function of the H concentration. The change in the concentration of trapping sites is equivalently described as a change in H solubility.[24] For a fixed H chemical potential, the concentration of occupied sites varies as the number of traps below the chemical potential. Hence, unlike electronic transport, under some situations, the density of binding sites varies with H concentration, temperature, and time.

Details of the trapping levels can be determined from the diffusion data as a function of temperature and concentration following the results in Ref. 13. Assuming the simple two-level density of states presented in Fig. 13, diffusion is given by

$$D_{\mathrm{eff}} = D_0 \exp\left(-\frac{E_A}{kT}\right), \tag{5}$$

with an activation energy E_A given by

$$E_A = \begin{cases} E_M - E_1 & \text{when } c < N_1 \\ E_M - E_{BC} & \text{when } N_1 + N_{BC} > c > N_1 . \end{cases} \tag{6}$$

This equation remains approximately valid not just for discrete levels but for broadened density of states which exhibit peaks in the occupied densities of states centered at the various band energies as well. Thus, as in Ref. 13, the energies of the shallow and deep trap levels can be determined from the activation energies of diffusion.

Furthermore, the position of $\mu_H(T)$ can be estimated using the following procedure. The diffusion is given by

$$D_{eff}=D_{micro}\exp\left(-\frac{[E_M-\mu_H(T)]}{kT}\right). \quad (7)$$

The microscopic diffusion prefactor is given by $D_{micro}=1/6\nu a^2$, where ν is the attempt frequency and a is the mean free path. With reasonable assumptions of $\nu\approx 10^{12}$ Hz and $a\approx 0.3$ nm, the microscopic diffusion prefactor amounts to $D_{micro}\approx 10^{-3}$ cm^2 s^{-1}. Assuming this prefactor, the energy in a Boltzmann factor necessary to yield the observed diffusion is computed using the relation

$$E_M-\mu_H(T)=-kT\ \ln\left(\frac{D_{eff}}{D_{micro}}\right). \quad (8)$$

This computed energy represents an estimate of the energy difference $E_M-\mu_H(T)$, which depends on the measurement temperature as well as material properties. The results depend only logarithmically on the assumed value of the microscopic prefactor so even an order of magnitude error will change the energies by less than 100 meV. Thus the approximate trap levels and the position of the hydrogen chemical potential can be estimated within the context of the two-band model using the time and temperature dependence of diffusion.

B. Temperature and concentration dependence of diffusion

The trap energies obtained by Eq. (6) are displayed in Fig. 3. For low D concentrations, the activation energy of the SSC material is approximately 1.7 eV, while for the LPCVD-grown poly-Si, the activation energy is about 0.4–0.5 eV. From the discussion above and from Ref. 13, we can conclude that the deep trap levels in SSC material are located about 1.7 eV below E_M. For the LPCVD material, the trap levels are about 0.5 eV below E_M. Apparently the traps in LPCVD grown poly-Si are significantly shallower than in SSC poly-Si for low concentration diffusion. Because the surface concentration is less than mid-10^{18} cm^{-3} for the SSC profiles, we can conclude that the trap concentration is above the mid-10^{18} cm^{-3} in SSC poly-Si. The LPCVD-grown material either has fewer traps, or these traps are inaccessible to the mobile hydrogen. These results are further confirmed in Sec. IV C by analysis of the spatial variation of the concentration profiles.

As the concentration of H increases above the deep trap levels, the activation energy shifts to the next peak in the occupied density of states. In the two-band model, this energy corresponds to the shallow trap levels at E_{BC}. From Fig. 3, E_{BC} is on the order of 0.4–0.6 eV below E_M in both LPCVD-grown and SSC poly-Si. This activation energy is quite similar in magnitude to the 0.48 eV observed for H diffusion in crystalline silicon.[23,25] The effective diffusion coefficient, determined from the high-D concentration peak in c-Si (Fig. 10) amounts to 2.2×10^{-14} cm^2 s^{-1} which is represented by the cross in Fig. 3. The effective diffusion from a plasma for c-Si and LPCVD-grown poly-Si is quite similar. In the crystalline silicon case, the activation energy of D_{eff} is believed to represent the energy difference between the migration saddle point and the Si-Si bond-centered position. Thus at high D concentrations, the diffusion appears to be independent of the disorder or structure of the silicon lattice. When large numbers of H are present in the silicon lattice, the average configurations available to most H atoms are the same independent of the lattice structure. The low-energy sites are occupied, leaving only the strong Si-Si bond sites available for binding. This suggests that the H platelets in c-Si may be prevalent and control diffusion in poly-Si as well.

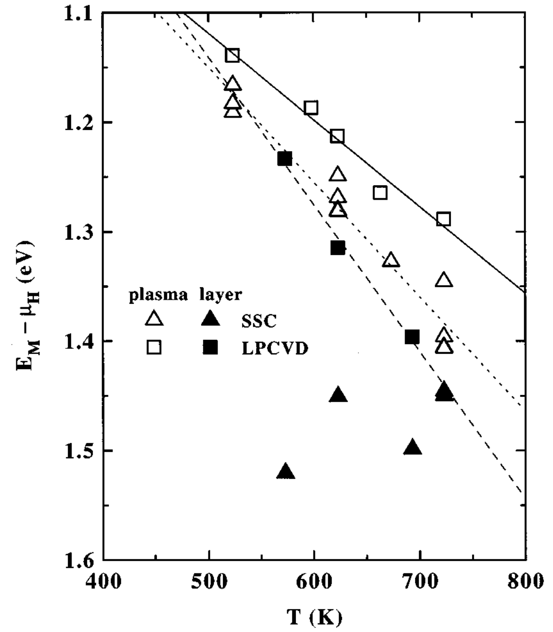

FIG. 14. The derived energy $E_M-\mu_H(T)$ vs measurement temperature, T for LPCVD layer diffusion (solid squares), LPCVD plasma diffusion (open squares), SSC layer diffusion (solid triangles), and SSC plasma diffusion (open triangles).

The position of the hydrogen chemical potential can be estimated assuming the microscopic prefactor is roughly 10^{-3} cm^2/s in Eq. (7). The results are shown in Fig. 14 as a function of the hydrogenation temperature for the various combinations of SSC and LPCVD-grown poly-Si and layer and plasma diffusion. Except for diffusion from a solid source into SSC poly-Si, which is represented by the solid triangles in Fig. 14, the chemical potential sinks deeper in energy with respect to E_M, roughly at the rate of 0.001 eV per K. Extrapolating the data in Fig. 14 to $T=0$ yields the activation energies presented in Fig. 3. This rate of change with temperature corroborates one major assumption of the two-level model. The hydrogen chemical potential cannot change rapidly with temperature if it resides in a large density of states. In order to exhibit the observed shift with temperature, the density of H trapping sites must be small at the hydrogen chemical potential. Therefore, the density of states must look approximately like the two-band model requires: two regions of high densities of states separated by a

deep minimum. The chemical potential in the SSC poly-Si is independent of temperature because μ_H is pinned in the large density of deep traps present in this material.

The temperature dependence of the hydrogen chemical potential has two possible origins. First, it may arise because there are more occupied states above the hydrogen chemical potential than unoccupied states below. The chemical potential usually moves away from energies of high densities of states toward low densities of states. Therefore, the data suggest that the hydrogen chemical potential is above a minimum in a density of states rather than below. A second explanation for the shift of E_M-$\mu_H(T)$ with temperature is that $\mu_H(T)$ in the solid is determined by the H quasichemical potential of the hydrogen plasma, μ_{plasma}, which decreases with increasing temperature. If we assume that hydrogen in the solid is in approximate equilibrium with the monatomic H in the plasma gas, then a decrease of μ_{plasma} causes an increase in E_M-$\mu_H(T)$. The quasichemical potential of the monatomic H gas is given by[26]

$$\mu_{plasma} = kT \ln(cV_Q), \quad (9)$$

where c is the concentration of atomic H, k is Boltzmann's constant, T is the gas temperature, and V_Q is the quantum volume which is equal to 10^{-24} cm^3 for H around room temperature.[26] The atomic H concentration c was measured to be about 5×10^{15} cm^{-3} (Ref. 12). Hence the rate of change of the hydrogen chemical potential with temperature is given by $\mu_{plasma}/T = -0.0016$ eV/K. This value depends only logarithmically on c, and on V_Q that is determined by fundamental constants. The decrease in chemical potential reflects the fact that at higher temperatures, H in the gaseous state is more favorable than H within the solid due to the greater entropy. The value agrees quite closely with the experimental value of -0.0013 ± 0.0002 eV/K and the direction with temperature. Therefore, the decrease in the hydrogen chemical potential could very likely arise from a decrease in the plasma chemical potential with temperature. Clearly, more work is needed to further illuminate the origin of the shift of μ_H with temperature.

Using the change of the hydrogen chemical potential versus temperature determined previously, we can correct the various data to compute E_M-$\mu_H(T)$ at a constant temperature. In Fig. 15, E_M-μ_H at $T=350$ °C is plotted as a function of the H concentration. For SSC poly-Si, E_M-$\mu_H(350$ °C) changes about 0.2 eV when the H concentration is increased above the mid-10^{18}-cm^{-3} level to about 10^{20} cm^{-3}. On the other hand, LPCVD-grown poly-Si shows only a small change of E_M-μ_H with increasing H concentration. Even at low H concentrations, hydrogen diffusion is dominated by shallow states rather than the deep states appearing in LPCVD-grown poly-Si. At low H concentrations there is a clear difference between H diffusion in LPCVD-grown and solid-state crystallized poly-Si.

A summary of the density of states information obtained in this section is presented in Fig. 13. The deep traps are present in appreciable concentrations only in SSC poly-Si and not in LPCVD-grown poly-Si. The deep traps are located roughly 1.5–1.7 eV below the transport level E_M. The hydrogen chemical potential resides about 1.2–1.3 eV below E_M. The hydrogen chemical potential does move about 0.2

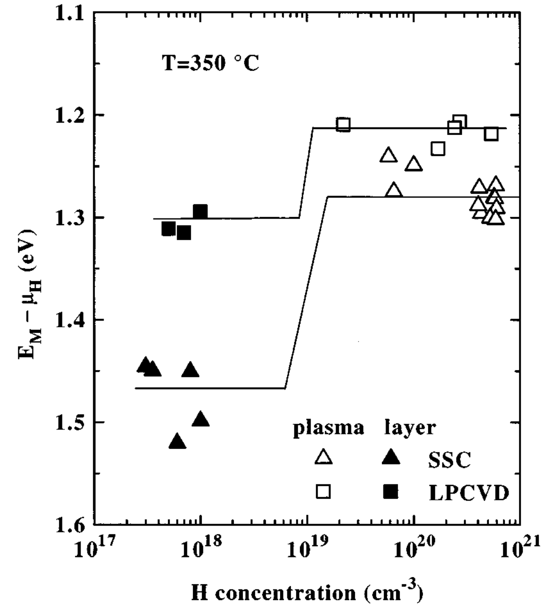

FIG. 15. $E_M-\mu_H(T)$ at 350 °C using the temperature dependence of $E_M-\mu_H(T)$ observed in Fig. 14 vs the peak concentration near the surface for LPCVD plasma (open squares), LPCVD layer (solid squares), SSC plasma (open triangles), and SSC layer (solid triangles).

eV, in response to changes in the H concentration from 10^{17} cm^{-3} to mid-10^{21} cm^{-3}. The depth of the shallow traps and high concentration diffusion are remarkably similar in the various forms of poly-Si and single-crystal silicon.

C. Spatial concentration profiles

Additional information about the H density of states can be obtained through analysis of spatial concentration profiles. If the free H concentration is comparable to or smaller than the deep trap concentration N_1, the diffusion is dominated by the deep traps and the deuterium profiles decay exponentially with depth. The concentration of traps N_1 is derived from the D depth profiles where the decay of the D concentration changes from an erfc to an exponential decay with depth. For H diffusion in SSC poly-Si (Figs. 1, 2, 5, and 6), N_1 is found to be about $5-8\times10^{18}$ cm^{-3}. The exponential slope x_0, which represents the mean free path between trapping events, is given by

$$x_0 = \frac{1}{\sqrt{4\pi r_k N_1}} \quad (10)$$

with r_k as the capture radius. From the observed value of $x_0\approx24$ nm the capture radius computes to $r_k\approx0.034$ nm, which is similar to that reported for a-Si:H.[14] On the other hand, for LPCVD-grown poly-Si, the mean free path x_0 is 75 nm, a value that is roughly three times larger than for SSC poly-Si. The trap density in LPCVD-grown poly-Si, however, is difficult to determine because no clear demarcation between exponential and erfc decay of the D concentration is observed. The trap concentration is either very small or very large if each trap has a very small effective capture radius. This absence of a deep trap signature in LPCVD grown

poly-Si is consistent with the low activation energy for layer diffusion discussed in Sec. IV B. A small increase in the H concentration greatly enhances diffusion when the trap density is low. Therefore, the density of sites with energies near the hydrogen chemical potential must be small suggesting that there are few traps in the LPCVD-grown poly-Si.

D. Time dependence of diffusion

The dependence of the effective diffusion coefficient on hydrogenation time presented in Fig. 4 suggests that relaxation times occur on time scales comparable to the experimental times. The time dependence of H diffusion is quite similar to that observed for H diffusion in amorphous silicon, as reported in Refs. 18 and 27. The power-law behavior in time is characteristic of exponential distributions of energy barriers for relaxation processes occurring during the diffusion process. These exponential distributions are quite generally observed in any material where the width of the distribution of energy barriers (kT_0) is broad compared to kT_{H}, where T_{H} is the hydrogenation or substrate temperature.[28] The dispersion parameter α is related to the ratio of the substrate-temperature disorder to the barrier disorder by the relation $\alpha = 1 - T/T_0 = 1 - \beta$.[29,30] Fitting the data in Fig. 4 to Eq. (3), we find that $T_0 \approx 830 \pm 50$ K. Thus the energetic disorder is characteristic of a temperature slightly below the crystallization temperature.

The energetic barriers may reflect H redistribution within a fixed density of binding sites, or redistribution of the silicon-hydrogen network in response to the altered H concentration. One example of the latter is the evolution of the H cluster-size distribution. As hydrogenation proceeds, the small clusters formed at short times are unstable to the formation of larger clusters. The time scale for a cluster of size N to disappear to be incorporated in a larger cluster is about N times longer than the time for a single H to diffuse from the small cluster to the neighboring larger clusters.[31]

E. Microscopic origins of H traps

The microscopic origin of the traps is difficult to determine. The density of traps in SSC poly-Si is within a factor of 3 of the number of spins in the material. One might expect, therefore, that the H is trapping at dangling-bond sites. While this trapping is energetically favorable and undoubtedly occurs, the H concentration necessary to passivate the dangling bonds greatly exceeds the number of Si dangling bonds by a factor of 50 or more.[6] Therefore, the dangling-bond sites must be competing with other more numerous sites for the H.

Another interesting fact to note is the relationship between the mean free paths x_0 and the grain size. In SSC material, the mean free path of $x_0 = 24$ nm is small compared to the grain size of 120 nm; while for LPCVD-grown poly-Si, the mean free path is 75 nm compared to the grain column diameter of 15 nm. Normally, the mean free path would be approximately equal to the grain size if the traps were associated with grain boundaries (Fig. 16). In the case of SSC poly-Si with randomly oriented grains, the small mean free path suggests that the traps are located within the interior of the grains. One could postulate various point defects such as vacancies, divacancies, and/or impurities as possible

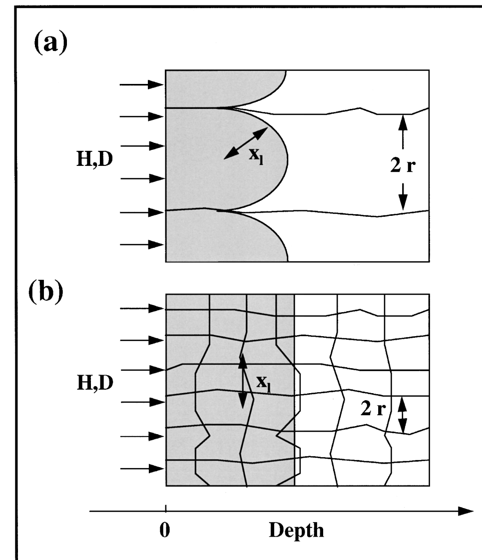

FIG. 16. Deuterium distribution in polycrystalline silicon assuming that (a) the diffusion length x_1 is small or (b) large compared to the average grain radius r.

H-trapping sites. On the other hand, the long mean free path of LPCVD-grown poly-Si compared with the grain diameter suggests that if traps are associated with the grain boundary, they are either in low concentrations or the H is guided away from the grain boundary in LPCVD-grown polycrystalline silicon. In the latter case each column acts like a diffusion pie. We can also conclude that the point defect traps occurring in SSC poly-Si are absent in LPCVD-grown material. Clearly a large-scale systematic investigation of H mean free path as a function of crystallite size, structure, and orientation would help to elucidate the connection between H traps and grain boundaries. These preliminary results suggest the relationship between traps and grain boundaries is not simple.

One promising idea is that the H traps around 1.5 eV arise from clustered H. Whenever the H concentration is large enough for clusters to exist, the effective diffusion will be controlled by trapping and release from such clusters. In low concentration diffusion and at low temperatures, the cluster-size distribution and therefore the trap energy and concentration remain roughly fixed. The profiles exhibit trapping, and the H concentration would not be directly connected to the reduction of spins. At higher temperatures and concentrations, the cluster-size distribution changes during the experiment, giving rise to changes in the trap density and time-dependent changes in the diffusion. The shallow sites represent strong and slightly strained Si-Si bond-center sites. In this case one would expect that hydrogenated platelets do not form in LPCVD-grown poly-Si, or that these sites are not accessible to migrating hydrogen. Although deuterium depth profiles show an accumulation of D in the surface which is indicative of hydrogenated platelets, TEM micrographs did no exhibit platelets in LPCVD-grown poly-Si.[20] This could be due to the limited resolution of the TEM technique which can only detect platelets exceeding 20 Å in length. Hence small platelets may still exist in the LPCVD-grown material. The formation of platelets must compete with the population of strong and slightly strained Si-Si bond-center sites. The

shallow states would dominate the H migration only when hydrogen is incorporated at concentrations higher than the deep-H trap densities.

V. SUMMARY

In summary, we have presented a detailed investigation on hydrogen/deuterium diffusion in solid-state crystallized and LPCVD-grown polycrystalline silicon. At high-D concentrations the diffusion is dispersive depending on exposure time. The dispersion is consistent with multiple trapping within a distribution of barriers between transport sites. Our data can be explained by a two-level model used to describe diffusion in hydrogenated amorphous silicon. Applying this model, information abut the H density-of-states distribution was obtained. The hydrogen chemical potential μ_H was found to reside about 1.2–1.3 eV below the migration saddle point E_M. μ_H moves about 0.2 eV in response to changes in the H concentration from 10^{17} to mid-10^{21} cm^{-3}. On the other hand, as the temperature increases, μ_H decreases. The shallow levels for hydrogen trapping are about 0.5 eV below the transport level, while the deep-H traps reside about 1.5–1.7 eV below E_M. At lower H concentrations, μ_H was found to depend markedly on the method used to prepare the poly-Si samples, a result due in part to the dependence of crystallite size on the deposition process. Clear evidence for deuterium deep traps was found only in the solid-state crystallized material. LPCVD-grown poly-Si displayed little evidence of deep trapping, and exhibited enhanced D diffusion compared to SSC poly-Si.

ACKNOWLEDGMENTS

This work was supported in part by NREL. One of the authors, N.H.N., is also pleased to acknowledge partial support from the Alexander von Humboldt Foundation, Federal Republic of Germany. The SIMS measurements were performed at the Materials Analysis Group of Philips in Sunnyvale, CA, and at Charles Evans & Associates in Redwood City, CA.

[1] N. H. Nickel, N. M. Johnson, and J. Walker, Phys. Rev. Lett. **75**, 3720 (1995).

[2] T. J. Kamins and P. J. Marcoux, IEEE Electron Device Lett. **EDL-1**, 159 (1980).

[3] A. Mimura, N. Konishi, K. Ono, J.-I. Ohwada, Y. Hosokawa, Y. A. Ono, T. Suzuki, K. Miyata, and H. Kawakami, IEEE Trans. Electron Devices **36**, 351 (1989).

[4] F. Boulitrop, A. Chenevas-Paule, and D. J. Dunstan, Solid State Commun. **48**, 181 (1983).

[5] R. Pandya and B. A. Khan, J. Appl. Phys. **46**, 5247 (1987).

[6] N. H. Nickel, N. M. Johnson, and W. B. Jackson, Appl. Phys. Lett. **62**, 3285 (1993).

[7] N. H. Nickel, N. M. Johnson, and W. B. Jackson, Phys. Rev. Lett. **71**, 2733 (1993).

[8] N. H. Nickel, N. M. Johnson, and C. G. Van de Walle, Phys. Rev. Lett. **72**, 3393 (1994).

[9] Y. V. Gorelkinskii and N. N. Nevinnyi, Pis'ma Zh. Tekh. Fiz. **13**, 105 (1987) [Sov. Tech. Phys. Lett. **13**, 45 (1987)].

[10] B. Holm, K. Bonde Nielsen, and B. Bech Nielsen, Phys. Rev. Lett. **66**, 2360 (1991).

[11] C. G. Van de Walle, P. J. H. Denteneer, Y. Bar-Yam, and S. T. Pantelides, Phys. Rev. B **39**, 10 791 (1989).

[12] N. M. Johnson, J. Walker, and K. W. Stevens, J. Appl. Phys. **69**, 2631 (1991).

[13] P. V. Santos and W. B. Jackson, Phys. Rev. B **46**, 4595 (1992).

[14] W. B. Jackson and C. C. Tsai, Phys. Rev. B **45**, 6564 (1992).

[15] H. M. Branz, S. E. Asher, and B. P. Nelson, Phys. Rev. B **47**, 7061 (1993).

[16] M. Kemp and H. M. Branz, Phys. Rev. B **47**, 7067 (1993).

[17] R. A. Street, C. C. Tsai, J. Kakalios, and W. B. Jackson, Philos. Mag. B **56**, 305 (1987).

[18] J. Shinar, R. Shinar, X. L. Wu, S. Mitra, and R. F. Girvan, Phys. Rev. B **43**, 1631 (1991).

[19] W. B. Jackson, N. M. Johnson, C. C. Tsai, I.-W, Wu, A. Chiang, and D. Smith, Appl. Phys. Lett. **61**, 1670 (1992).

[20] N. H. Nickel (unpublished).

[21] R. G. Wilson, F. A. Stevie, and G. W. Magee, *Secondary Ion Mass Spectrometry—A Practical Handbook for Depth Profiling and Bulk Impurity Analysis* (Wiley, New York, 1989).

[22] D. E. Carlson and C. W. Magee, Appl. Phys. Lett. **33**, 81 (1978).

[23] A. Van Wieringen and N. Warmholtz, Physics **22**, 849 (1956).

[24] W. Beyer, J. Non-Cryst. Solids (to be published).

[25] C. H. Seager, R. A. Anderson, and J. K. G. Panitz, J. Mater. Res. **2**, 96 (1987).

[26] C. Kittel, *Thermal Physics* (Wiley, New York, 1969), p. 164.

[27] W. Beyer and H. Wagner, in *Amorphous Silicon Technology–1994*, edited by E. A. Schiff, M. Hack, A. Madan, M. Powell, and A. Matsuda, MRS Symposia Proceedings No. 336 (Materials Research Society, Pittsburgh, 1994), p. 323.

[28] S. Taraskin, J. Non-Cryst. Solids **137&138**, 25 (1991).

[29] J. Kakalios, R. A. Street, and W. B. Jackson, Phys. Rev. Lett. **59**, 1037 (1987).

[30] J. Shinar, R. Shinar, S. Mitra, and J.-Y. Kim, Phys. Rev. Lett. **62**, 2001 (1989).

[31] W. B. Jackson, P. V. Santos, and C. C. Tsai, Phys. Rev. B **47**, 9993 (1993).